Journal of Power Sources 241 (2013) 502–508

Contents lists available at SciVerse ScienceDirect

Journal of Power Sources

journal homepage: www.elsevier.com/locate/jpowsour

Influence of B_2O_3 addition on the ionic conductivity of $Li_{1.5}Al_{0.5}Ge_{1.5}(PO_4)_3$ glass ceramics

Harsharaj S. Jadhav [a], Min-Seung Cho [a], Ramchandra S. Kalubarme [a], Jong-Sook Lee [a], Kyu-Nam Jung [b], Kyoung-Hee Shin [b], Chan-Jin Park [a,*]

[a] Department of Materials Science and Engineering, Chonnam National University, 77, Yongbong-ro, Buk-gu, Gwangju 500-757, Republic of Korea
[b] Energy Storage Department, Korea Institute of Energy Research, 152, Gajeongro, Yuseonggu, Daejeon 305-343, Republic of Korea

HIGHLIGHTS

- B_2O_3 added LAGP glass ceramics were prepared by melt-quenching method.
- Effect of B_2O_3 addition on ionic conductivity of LAGP glass ceramics was studied.
- Stability of B_2O_3 added LAGP glass ceramics in aqueous electrolytes was studied.

ARTICLE INFO

Article history:
Received 21 February 2013
Received in revised form
15 April 2013
Accepted 27 April 2013
Available online 10 May 2013

Keywords:
Glass ceramic
Impedance analysis
Ionic conductivity
Chemical stability

ABSTRACT

The effects of B_2O_3 addition on the properties of the $Li_{1.5}Al_{0.5}Ge_{1.5}(PO_4)_3$ (LAGP) glass ceramic have been studied. The crystallization temperature of the LAGP decreases with the addition of B_2O_3. The glasses are crystallized at different temperatures and characterized for microstructure and ionic conductivity. The highest total conductivity of the glass ceramic material, 6.9×10^{-4} S cm^{-1} at 25 °C is achieved by crystallizing the glass at 825 °C for 5 h with the addition of 0.05 wt% B_2O_3. Non-linearity in Arrhenius plot is observed due to the characteristics of $AlPO_4$ dielectric phase. In addition, the B_2O_3 added LAGP glass ceramic is stable in weak acidic and neutral solutions, but highly corroded in strong acidic and basic solutions.

1. Introduction

Rechargeable Li-ion batteries are key components in our current, information-rich world [1]. They have been used as energy sources for a variety of electronic devices used daily for communication and tasks because of their high energy densities. However, to drive an electric vehicle over a long distance in a single charge, the energy density of state-of-the-art Li-ion technology is insufficient. On the other hand, Li-air batteries have 3–5 times higher gravimetric energy density than conventional Li-ion batteries, so if commercialized, they would dramatically improve the driving distance of electric vehicles (EV) [2]. The high energy densities of both battery systems have been resulted from a high operation voltage. Hence, flammable organic solvents have been exclusively used in these batteries as electrolytes, because they can tolerate such high voltages. In some cases, organic electrolytes have caused serious safety problems in Li-ion batteries such as fire hazards and electrolyte leakage, calling for the need to replace currently used organic carbonate liquid solutions with safer and more reliable electrolytes [3]. In order to overcome the safety issues, researchers have employed polymers [4,5], and ceramics [6–8] as electrolytes for rechargeable Li-ion batteries. In particular, all solid state batteries with ceramic solid electrolytes have been recognized as ultimate safe batteries. However, to make solid-state Li-ion batteries of efficient design and high performance, a solid lithium ion conductor with a total conductivity above 10^{-3} S cm^{-1} is desirable [9].

Some crystalline glass ceramics, known as LISICON (Lithium super ionic conductor), exhibit ionic conductivity comparable to those of liquid electrolytes. These are the Lithium-analogues of NASICON type glass ceramics like lithium-aluminium-titanium-phosphate (LATP) [10] and lithium-aluminium-germanium-phosphate (LAGP) [11], and they are good candidate as

* Corresponding author. Tel.: +82 92 530 1704; fax: +82 62 530 1699.
E-mail address: parkcj@jnu.ac.kr (C.-J. Park).

0378-7753/$ – see front matter © 2013 Elsevier B.V. All rights reserved.
http://dx.doi.org/10.1016/j.jpowsour.2013.04.137

electrolytes for all solid state lithium-ion batteries. In addition to the ionic conductivity, the surface of a solid electrolyte should be stable in contact with other components for longer lifetime of battery. The solid electrolyte should be stable in contact with lithium, water and electrolytes containing Li-salts if it is to be used as a protective layer in all solid state batteries.

The LAGP glass ceramic has been reported to exhibit superior stability in contact with lithium metal [12], but lower ionic conductivity than that of a liquid electrolyte ($\sim 10^{-3}$ at room temperature) [13,14]. Therefore, the insufficient conductivity of the LAGP needs to be improved. There have been reports on the preparation of LAGP by melt-quenching [15], solid solution [16] and sol–gel [17] methods. For the LAGP made by melt-quenching processes, the temperature and duration of time required for crystallization were reported to be 850 °C and 12 h respectively [12,15]. One way to decrease the crystallization temperature is to add sintering aids that have low melting points and make liquid phases at comparatively lower temperatures. In addition, the liquid phases promote densification and coarsening at lower temperatures. Low temperature crystallization with sintering aids reduces dielectric properties, because the dielectric constants of the sintering aids are lower than that of the ceramic. Furthermore, the reaction between the sintering aid and ceramic causes the formation of a secondary phase with a low dielectric constant [18]. However, some sintering aids improve dielectric properties as they incorporate into the ceramic grain and suppress the formation of the secondary phase [19].

The present study investigates the effects of B_2O_3 as sintering aid on the thermal properties, crystallization behaviour, microstructure and ionic conductivity of the LAGP glass ceramic. Since B_2O_3 has a flat 6-numbered ring structure formed of boron and oxygen, its structure is more open than the open tetrahedron structure of quartz glass, and it is favourable for ion conductivity [20].

2. Experimental

The melt-quenching method was used to prepare the LAGP and B_2O_3-added LAGP ceramics. B_2O_3 of 0.05, 0.1, 0.2 and 0.4 wt% was added to pristine LAGP ($Li_{1.5}Al_{0.5}Ge_{1.5}(PO_4)_3$), respectively. The starting precursor materials viz. Li_2CO_3, Al_2O_3, GeO_2, B_2O_3 and $NH_4H_2PO_4$ were mixed in mortar and then ball milled further for 1 h for homogenization. The milled batch was transferred to the electric furnace for melting. Initially, the furnace was heated to 350 °C at a rate of 1 °C min^{-1} and held at that temperature for 1 h to release volatile components. Then, the furnace was heated to 1250 °C at the same rate and held for another 2 h. A clear, homogeneous and viscous melt was poured onto a preheated (150 °C) stainless steel plate and quickly pressed by another steel plate to yield transparent glass. Furthermore, the obtained transparent glass was annealed for 2 h at 500 °C to release the thermal stresses and then cooled to room temperature. After the heat treatment, the annealed glass specimens were crystallized for 5 h at various temperatures from 800 to 850 °C. The LAGP glass ceramics, in which various B_2O_3 concentrations of 0 wt%, 0.05 wt%, 0.1 wt%, 0.2 wt% and 0.4 wt% were added, were named as B_0, $B_{0.05}$, $B_{0.1}$, $B_{0.2}$ and $B_{0.4}$ respectively.

Differential thermal analysis (DTA) was conducted to investigate the effect of B_2O_3 addition on the crystallization temperature of LAGP. The content of Li, Al, Ge, P and B in the specimen was measured by using inductively coupled plasma atomic emission spectroscopy (ICP-AES). X-ray diffraction (XRD) patterns of all specimens were obtained using the Rigaku-D/MAX-Ultima III-600 X-ray diffractometer operated at voltage of 40 kV and current of 40 mA with Cu Kα radiation in the 2θ range from 2° to 80° with a 0.02° step size and step scan of 0.3s. Crystalline phases were identified by comparing the observed data with the standards from International Center for Diffraction Data. Scanning electron microscope (SEM) images were obtained using Hitachi S-4700 FE-SEM. The AC impedance measurements of all the crystallized samples were carried out using the ZIVE SP2 instrument in the 1 Hz to 1 MHz frequency range at voltage amplitude of 100 mV. Samples for AC impedance measurement were polished to obtain uniform thickness and flat surfaces. Further, the opposite faces were coated with Ag paint for good electrical contact. Ag paint was dried at room temperature in dry atmosphere for several hours. The good electrical conductivity of coated surface was ensured before loading the samples in the setup for conductivity measurements. The Ag coated specimens were assembled into a cell using stainless steel (SS) blocking electrode in a cell fixture. The fixture containing the SS/Ag/glass ceramic/Ag/SS cell was subsequently placed in a stable fixture holder with attached electrical connection leading to the impedance spectrometer. The conductivity of specimens was computed from the ac impedance spectra. *Z* plot and Z view software was employed for impedance data acquisitions analysis. The impedance spectra show normally one semicircle at room temperature (25 °C). The diameter of the semicircle was further normalized with respect to the thickness and cross-sectional area of the specimens to obtain the total conductivity of the specimens.

3. Result and discussion

Fig. 1(a) shows the DTA curves obtained for LAGP and B_2O_3 added LAGP glasses in the temperature range of 200–700 °C at the heating rate of 10 °C min^{-1}. The glass crystallization temperature

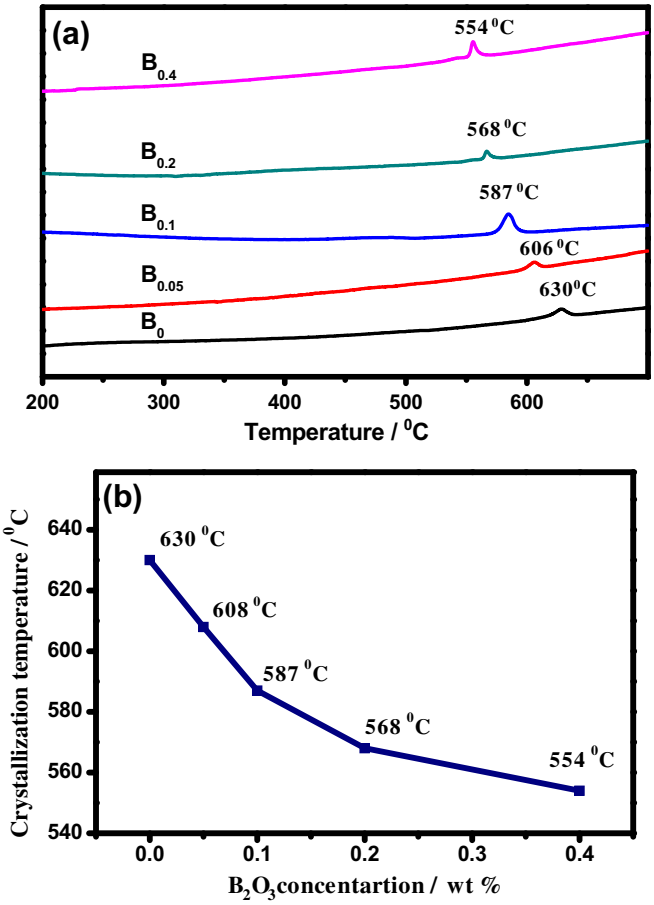

Fig. 1. (a) DTA plot for B_0 (0 wt% B_2O_3), $B_{0.05}$ (0.05 wt% B_2O_3), $B_{0.1}$ (0.1 wt% of B_2O_3), $B_{0.2}$ (0.2 wt% of B_2O_3) and $B_{0.4}$ (0.4 wt% of B_2O_3) samples. (b) The variation of crystallization temperature with the different B_2O_3 addition.

(T_c) decreased gradually with increasing B_2O_3 addition in the LAGP. The decrease in T_c by the addition of B_2O_3 suggests that the glass crystallized more easier with addition of B_2O_3. For the pristine LAGP, the crystallization temperature was 630 °C but it decreased to 554 °C for $B_{0.4}$ as shown in Fig. 1(b). This result suggests that B_2O_3 can be used as a sintering aid in solid glass ceramic formation.

The chemical composition of the glass ceramics were obtained from the ICP-AES measurement and summarized in Table 1.From the result it is observed that the amount of Li, Ge, Al and P is nearly same for all the composition and independent of the boron (B) addition. However the B content is less than the added amount. This might be due to evaporation during melting and crystallization process of glass ceramic.

The morphologies of the glass ceramics sintered for 5 h at different temperatures were examined by FE-SEM and the images are shown in Fig. 2. In the images, morphology was presented as a function of B_2O_3 addition and sintering temperature. For the pristine B_o specimen, crystallization started at 800 °C, and the glass ceramics having a well crystallized microstructure was obtained at the sintering temperature of 850 °C which is approximately 200 °C higher than the crystallization temperature revealed by the DTA curve. For the $B_{0.05}$ specimen, crystallization started at 775 °C and continued with increasing temperature, resulting in improved crystallinity. In addition, the grains showed better connection among themselves due to the mainly segregation of B_2O_3 in the grain boundaries (Fig. 3). Further increase in temperature caused the sintering of the grains and the increase of impurities in the form of needles on the surface. In addition, the grain size of the $B_{0.05}$ glass ceramic increased to 0.8–1.5 μm from that of the B_0. The increase in grain size is attributed to the liquefaction of the grain boundaries resulting from the addition of B_2O_3. The melting point of B_2O_3 is about 450 °C, which is much lower than the temperature used for the crystallization process. Therefore, the liquid phase in grain boundaries facilitated the rearrangement of the grains during the crystallization process. However, for the $B_{0.1}$ specimen, the grain size decreased with further addition of B_2O_3. On the other hand, the $B_{0.2}$ specimens treated at various temperatures exhibited crystalline morphology. When the B_2O_3 addition exceeds a certain wt%, B_2O_3 may exist independently as well as in the solid solution. Furthermore, the addition of 0.4% B_2O_3 resulted in the crystallization of the specimen at 800 °C. Decreased in the B_2O_3 content on the glass surface was observed for the specimen ($B_{0.4}$) crystallized at 850 °C due to evaporation of the B_2O_3 liquid phase during the crystallization process [21].

A typical room temperature impedance plot for the $B_{0.05}$ specimen crystallized for 5 h at 825 °C is illustrated in Fig. 4. The impedance spectra show a pattern with significant curvature that intersects the Im Z axis towards the high frequency side, which is interpreted as circuit resistance (R_s) external to the specimen. Starting from the intersection and going towards the lower frequency side, a depressed semicircle is observed. The semicircle segments are followed by Warburg-type impedance at low frequencies associated with the diffusion process. The experimental spectra were fitted by using the equivalent circuit previously suggested by J.S. Thokchom et al. as shown in the inset of Fig. 3 [22].

Table 1
Chemical analysis data for of $Li_{1.5}Al_{0.5}Ge_{1.5}(PO_4)_3$–$xB_2O_3$ ($x = 0.0$–0.4) glass ceramic.

Specimen	Chemical formula LAGP	Total B content (wt%)
B_0	$Li_{1.47}Al_{0.49}Ge_{1.49}(PO_4)_{2.97}$	0
$B_{0.05}$	$Li_{1.48}Al_{0.50}Ge_{1.48}(PO_4)_{2.96}$	0.092
$B_{0.1}$	$Li_{1.47}Al_{0.48}Ge_{1.47}(PO_4)_{2.98}$	0.188
$B_{0.2}$	$Li_{1.46}Al_{0.48}Ge_{1.47}(PO_4)_{2.97}$	0.390
$B_{0.4}$	$Li_{1.47}Al_{0.49}Ge_{1.48}(PO_4)_{2.98}$	0.788

The existence of single semicircle was observed for $B_{0.05}$, representing the total resistance (R_t) of the specimen. The total resistance of a specimen (R_t) is the sum of the grain resistance (R_g) and the grain boundary resistance (R_{gb}). The total resistance ($R_t = R_g + R_{gb}$) of a specimen at a particular temperature was further normalized with respect to the cross-sectional area and thickness of the specimen to calculate the total conductivity (σ_t).

The variation in the conductivity of the LAGP glass ceramic as a function of the B_2O_3 addition and crystallization temperature is shown in Fig. 5(a). The total ionic conductivity was calculated by using following equation:

$$\sigma = \frac{t}{A} \times \frac{1}{R} \quad (1)$$

where t, A and R are the thickness, area and resistance of the specimen respectively. From the plot, it was found that the ionic conductivity of the glass ceramic was enhanced by the addition of the B_2O_3 into the LAGP. This enhancement was attributed to the presence of B_2O_3 at the grain boundaries, which enhanced the Li-ion diffusion process. The conductivity also increased with the increase of crystallization temperature up to 825 °C and decreased with further increase, which might be due to the increase in secondary dielectric $AlPO_4$ phases in the specimen. The presence of dielectric phase ($AlPO_4$) along the grain boundaries leads to the decrease in the ionic conductivity of a specimen [22]. In contrast, highest conductivities of 1.22×10^{-4} S cm^{-1} for the B_0 sample and 2.01×10^{-4} S cm^{-1} for the $B_{0.4}$ sample were obtained when the samples were crystallized at 850 °C and 800 °C, respectively. These results indicate that the crystallization temperature decreased from 850 °C to 800 °C with increasing B_2O_3 addition in the LAGP. These results are also in good agreement with the DTA results. DTA data shown in Fig. 1 indicated that the crystallization temperature decreased from the addition of B_2O_3 into LAGP.

Among the pristine and the B_2O_3 added LAGP samples, the $B_{0.05}$ LAGP sample crystallized at 825 °C showed the highest ionic conductivity of 6.94×10^{-4} S cm^{-1}. Typical impedance plots of the specimens at their highest conductivities are shown in Fig. 5(b). With the increase in B_2O_3 addition in LAGP from 0.05 to 0.4 wt%, the total resistance of the specimen increased from 800 Ω to 2416 Ω.

The B_0 (850 °C), $B_{0.05}$ (825 °C), $B_{0.1}$ (825 °C), $B_{0.2}$ (825 °C) and $B_{0.4}$ (800 °C) specimens which showed the highest conductivity were examined for structural analysis. The XRD patterns of specimens crystallized for 5 h at 850 °C (B_0) and 825 °C ($B_{0.05}$, $B_{0.1}$ and $B_{0.2}$) and 800 °C ($B_{0.4}$), are shown in Fig. 6. The NASICON-type phase of $LiGe_2(PO_4)_3$ was found to be the major crystalline phase, along with the Li_2O and $AlPO_4$ secondary phases in the B_0, $B_{0.05}$, $B_{0.1}$, $B_{0.2}$ and $B_{0.4}$ glass ceramics. However, the peaks corresponding to B_2O_3 were not found in XRD patterns due to its amorphous nature. Both secondary phases, Li_2O and $AlPO_4$, are considered to concentrate in the grain boundary region and to constrain the movement of Li-ions. Accordingly, the ionic conductivity of the glass ceramic is degraded. Fig. 6 shows no significant change in $AlPO_4$ impurity intensity of XRD patterns with increased addition of B_2O_3 content from 0.05 to 0.4 wt%.

From the total conductivity graph shown in Fig. 5, the specimens with the highest ionic conductivity in each batch of sample were explored to investigate the influence of operating temperature on the ionic conductivity of LAGP glass ceramic. All the specimens were tested in the temperature range of −20 to 80 °C. Fig. 7 shows the Arrhenius plots for total conductivities (σ_t) of the specimens crystallized for 5 h at 850 °C (B_0), 825 °C ($B_{0.05}$, $B_{0.1}$ and $B_{0.2}$) and 800 °C ($B_{0.4}$). The Arrhenius plots for the specimens were nonlinear and exhibited the two linear segments intersecting at about 40 °C. The nonlinearity appears to be attributed to the

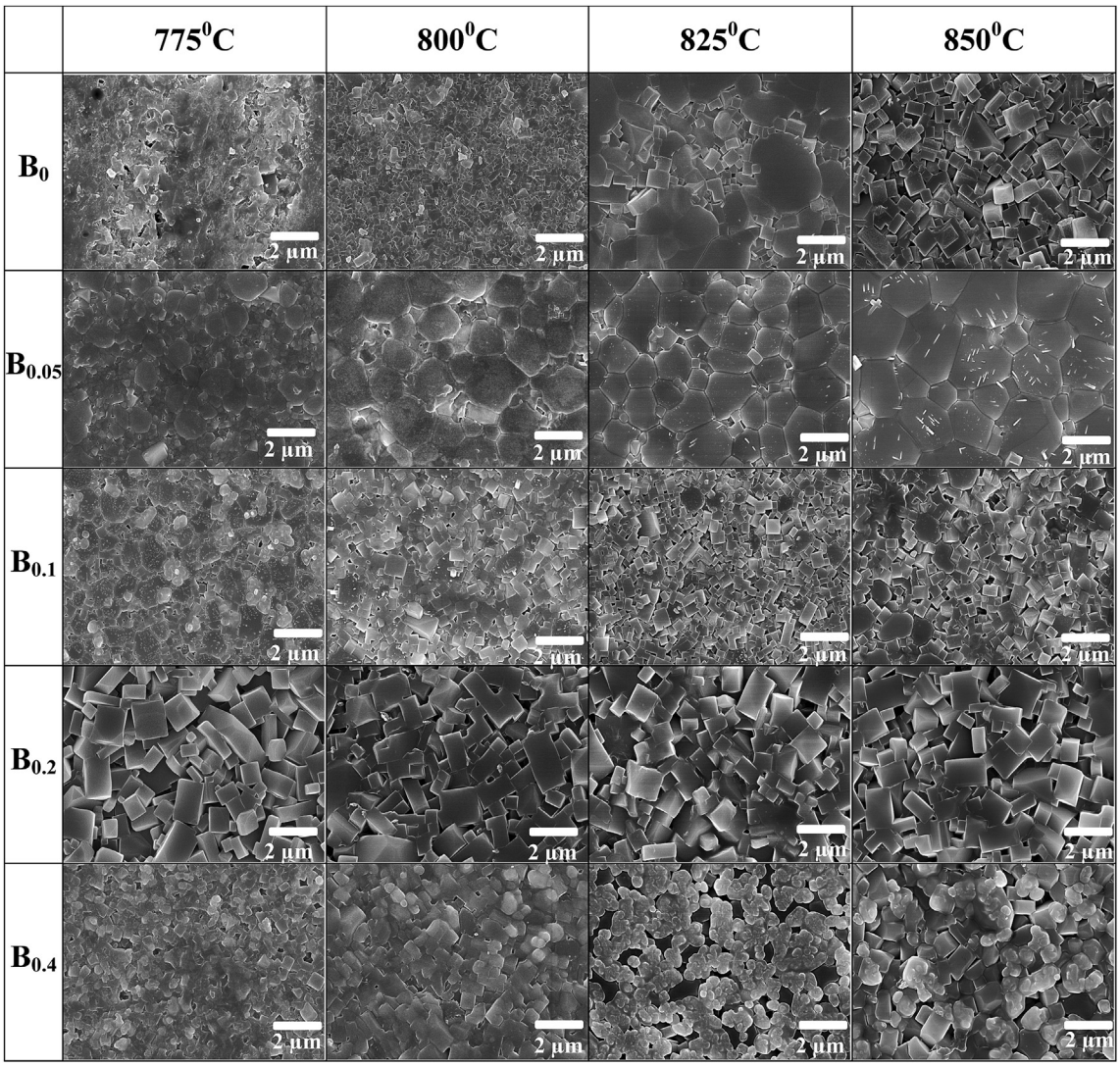

Fig. 2. FE-SEM images for B_0, $B_{0.05}$, $B_{0.1}$, $B_{0.2}$ and $B_{0.4}$ specimens crystallized at different temperatures ranging from 775 to 850 °C.

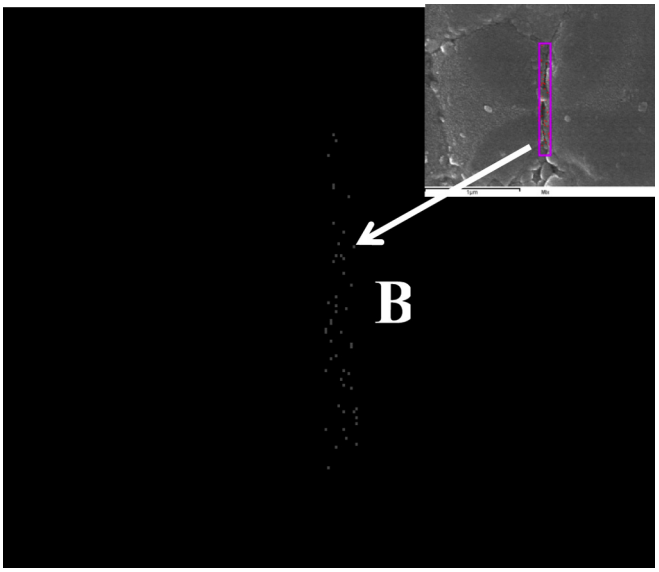

Fig. 3. EDS mapping of B content along the grain boundary.

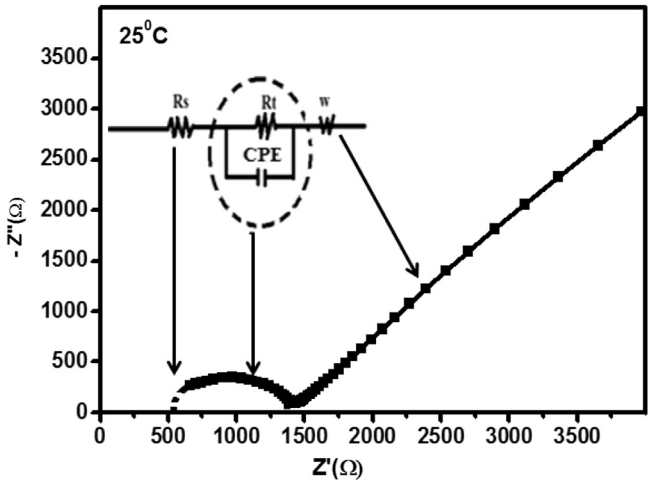

Fig. 4. AC impedance spectra of $B_{0.05}$ specimens crystallized for 5 h at 825 °C. Inset is the equivalent circuit used to fit the curve.

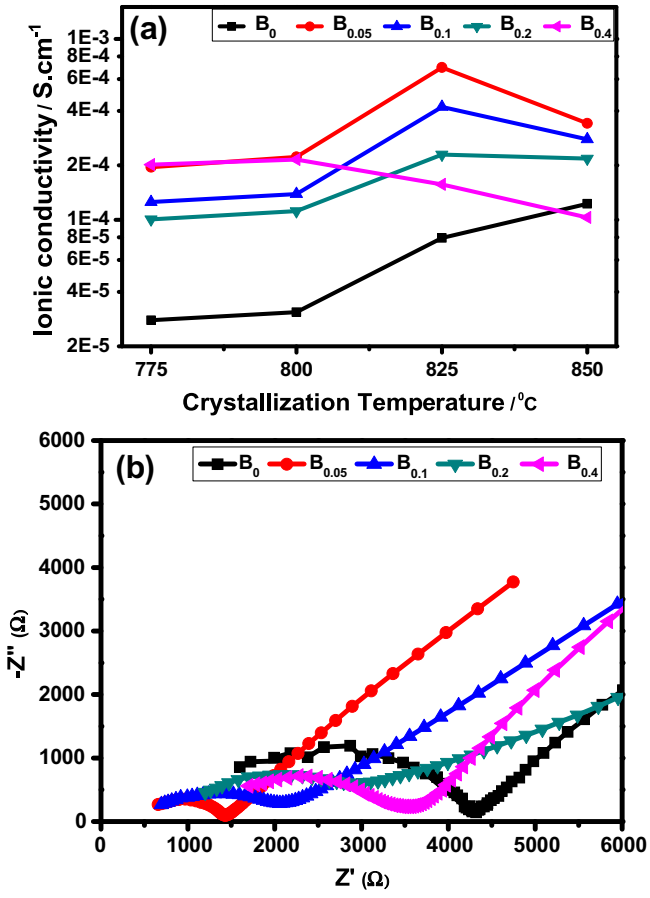

Fig. 5. (a) Total ionic conductivity plots (σ_t) for the B_0, $B_{0.05}$, $B_{0.1}$, $B_{0.2}$ and $B_{0.4}$ specimens crystallized for 5 h at 775, 800, 825 and 850 °C. (b) Impedance plots for specimens crystallized for 5 h at 850 °C (B_0), 825 °C ($B_{0.05}$, $B_{0.1}$ and $B_{0.2}$) and 800 °C ($B_{0.4}$).

presence of impurity phases, $AlPO_4$ and Li_2O in the grain boundaries. The linear regions of all five specimens fitted to the Arrhenius equation as expressed by

$$\sigma = A \exp\left(-\frac{E_a}{kT}\right) \quad (2)$$

where A is the pre-exponential factor, E_a is the activation energy and k is the Boltzmann constant.

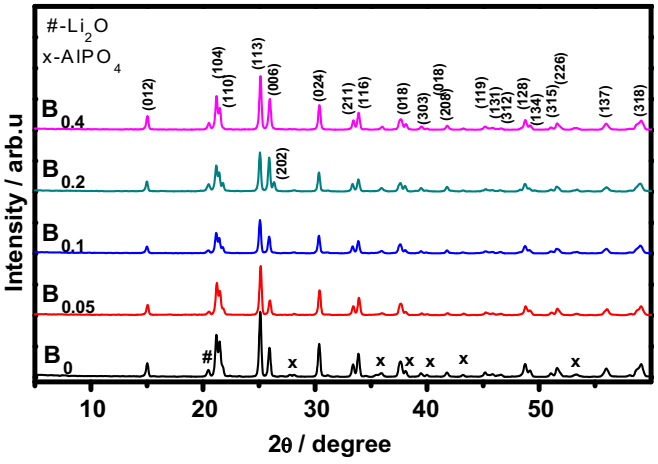

Fig. 6. XRD patterns for the specimens crystallized for 5 h at 850 °C (B_0), 825 °C ($B_{0.05}$, $B_{0.1}$ and $B_{0.2}$) and 800 °C ($B_{0.4}$).

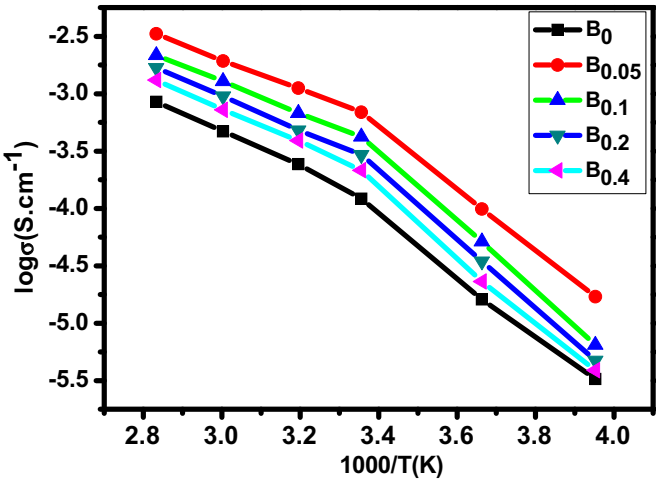

Fig. 7. Arrhenius plots for total ionic conductivities (σ_t) of the specimens crystallized for 5 h at 850 °C (B_0), 825 °C ($B_{0.05}$, $B_{0.1}$ and $B_{0.2}$) and 800 °C ($B_{0.4}$).

The $B_{0.05}$ specimen crystallized for 5 h at 825 °C showed the highest total conductivity (σ_t) over the entire temperature range. The ionic conductivities of specimens ranged from 10^{-5} to 10^{-3} S cm^{-1}. The LAGP glass ceramic without B_2O_3 addition exhibited lower total ionic conductivity than the LAGP glass ceramics with B_2O_3. Nevertheless, the total conductivity of the LAGP samples with B_2O_3 addition, decreased with increasing B_2O_3 addition above 0.05 wt%. The degradation of the conductivity with the increase in B_2O_3 addition appears to be associated with grain boundary shape. According to Fig. 2, the LAGP samples with higher B_2O_3 addition had more distinct grain boundaries. These grain boundary regions are highly resistive, obstructing the Li ion transportation. In addition, the slope in the Arrhenius plots in the high temperature region (>40 °C) decreased for all specimens, which appears to be attributed to the decomposition of the primary crystalline phase and the formation of $AlPO_4$ at the grain boundaries of the specimens. Adsorption and desorption of the Li^+ onto dielectric ($AlPO_4$) surface in grain boundary region leads to the formation of space charge effect. The inflection point (40 °C) in the Arrhenius plots depends on the stability of $AlPO_4$: Li^+ complex. Above 40 °C $AlPO_4$: Li^+ destroyed and Li^+ diffused away from the grain boundaries, which results in reduction ionic conductivity in the high temperature region (>40 °C) [22]. As listed in Table 2, the activation energies were calculated from two lines in the Arrhenius plots below and above the inflection temperature (40 °C) for the specimens crystallized for 5 h at 850 °C (B_0), 825 °C ($B_{0.05}$, $B_{0.1}$ and $B_{0.2}$) and 800 °C ($B_{0.4}$). The low temperature activation energy ranges from 21.6 to 24.9 kJ mol^{-1} which represent space charge mediated transport of lithium ion conduction [23]. High temperature activation energy ranges from 10.8 to 12.3 kJ mol^{-1} and characterize the energy barrier associated with the transport of

Table 2
Activation energies of LAGP glass ceramic crystallized at 850 °C (B_0), 825 °C ($B_{0.05}$, $B_{0.1}$ and $B_{0.2}$) and 800 °C ($B_{0.4}$) for 5 h.

Specimen	Activation energy, E_{a1} (kJ mol^{-1}) (−20 to 40 °C)	Activation energy, E_{a2} (kJ mol^{-1}) (40–80 °C)
B_0	24.9	12.2
$B_{0.05}$	21.6	10.8
$B_{0.1}$	23.2	11.3
$B_{0.2}$	24.9	12.1
$B_{0.4}$	24.3	12.3

lithium ion through the crystalline structure of LAGP [12]. While the $B_{0.05}$ samples exhibited relatively smaller activation energy than other samples. This might be due to their formations of a well-developed crystal structure [22].

For the application of the glass ceramics as electrolytes, it is necessary to check the stability and durability of the glass ceramics in acidic and alkaline solutions. The $B_{0.05}$ glass ceramic showing the best microstructure and highest ionic conductivity was further investigated for the stability and durability tests. The stability of the $B_{0.05}$ glass ceramic was evaluated by keeping the in deionized water and aqueous 1 M $LiNO_3$, 1 M LiCl, 1 M LiOH and 0.1 M HCl for 3 weeks at 25 °C. The pH values of the solutions were 7 for the deionized water, 6 for 1 M for $LiNO_3$ solution, 6 for 1 M LiCl solution, 14 for 1 M LiOH solution and 1 for 0.1 M HCl solution. Fig. 8 shows the low magnification SEM images of the $B_{0.05}$ specimens before and after 3 weeks immersion tests in different aqueous solutions. The high magnification images of the specimens after the tests are given in the insets of respective specimen SEM images. The specimen immersed in deionized water exhibits compact morphology with some surface dissolution. In contrast, the specimens immersed in 1 M $LiNO_3$ and 1 M LiCl show the dissolution of the glass ceramic along the grain boundaries. The high magnification images for these specimens show the presence of small pores. The pitting effect is more pronounced in the presence of Cl^- ions compared to NO^{3-} ions, because chlorine ions are more corrosive than nitrate ions. Hence more rough surface were formed for samples immersed in the 1 M LiCl than the samples immersed in 1 M $LiNO_3$ having same pH value. The specimens immersed in 1 M LiOH and 0.1 M HCl show significant changes in morphology after immersion for 3 weeks. Thus, it can be concluded that the $B_{0.05}$ glass ceramic is unstable in strong acidic and alkaline media, but can be acceptable in neutral and weak alkaline/acidic media.

Fig. 9 shows the XRD patterns of the $B_{0.05}$ solid glass ceramics immersed in deionized water and aqueous solutions for 3 weeks. The $B_{0.05}$ glass ceramic immersed in deionized water and 1 M $LiNO_3$ show no significant changes in their XRD patterns from those of the pristine with $B_{0.05}$ exhibiting NASICON type structure. This result indicated that $B_{0.05}$ was stable and durable for a long period of time

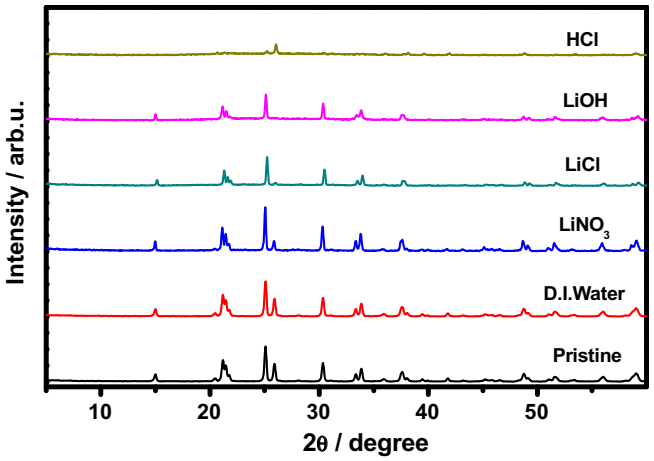

Fig. 9. X-ray diffraction patterns of the pristine $B_{0.05}$ and the $B_{0.05}$ immersed for 3 weeks in deionized water, 1 M $LiNO_3$ solution, 1 M LiCl solution, 1 M LiOH solution and 0.1 M HCl solution at 25 °C.

in the deionized water and in the $LiNO_3$ solution. The XRD patterns of the $B_{0.05}$ solid glass ceramics immersed in aqueous 1 M LiOH and 1 M LiCl solutions exhibited the notable decrease in peak intensities, and some peaks even disappeared. This indicates that the glass ceramics corroded in alkaline solutions. The glass ceramic immersed in 0.1 M HCl became almost amorphous, indicating the high corrosive nature of HCl and the instability of the glass ceramic in highly acidic environment. These results demonstrate that the $B_{0.05}$ specimen is unstable in strong acidic and strong basic environments and cannot be employed as an electrolyte with strong acidic or alkaline solution.

Furthermore, the total conductivity of the $B_{0.05}$ specimen was measured after the stability tests and the results are shown in Fig. 10. Changes in the microstructure during the stability test induced changes in the conductivity of the $B_{0.05}$ specimens. The total conductivity and pH values of the solutions used for stability tests are shown in Table 3. The total conductivity of the $B_{0.05}$ glass

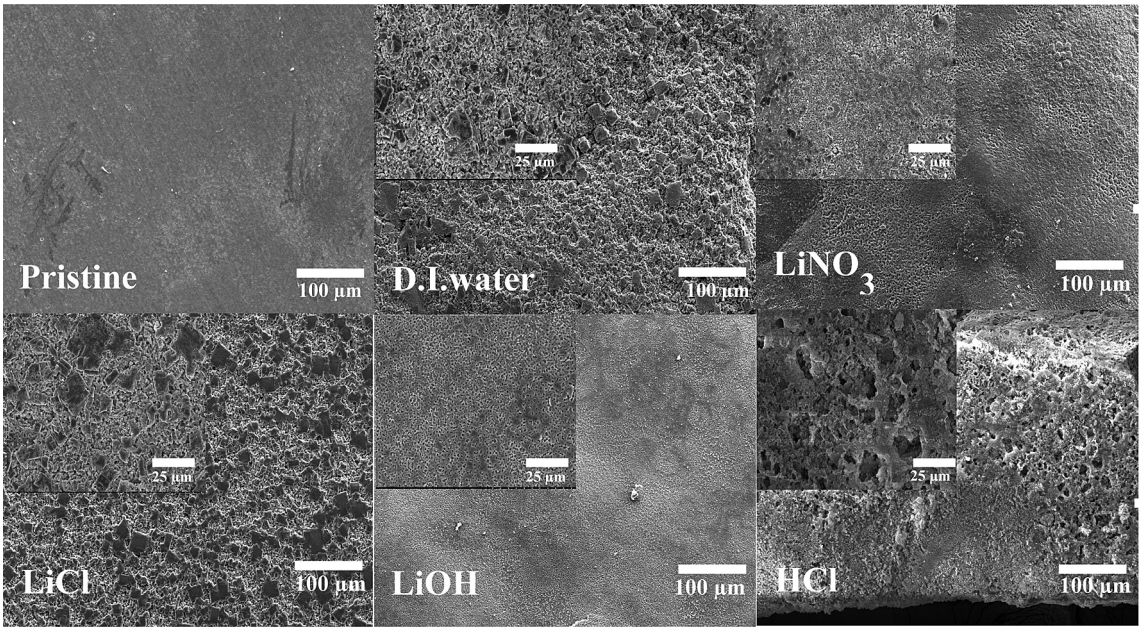

Fig. 8. SEM images of pristine $B_{0.05}$ and $B_{0.05}$ specimens immersed for 3 weeks in distilled water, 1 M $LiNO_3$ solution, 1 M LiCl solution, 1 M LiOH solution and 0.1 M HCl solution at 25 °C. Inset shows high magnification images of the respective samples.

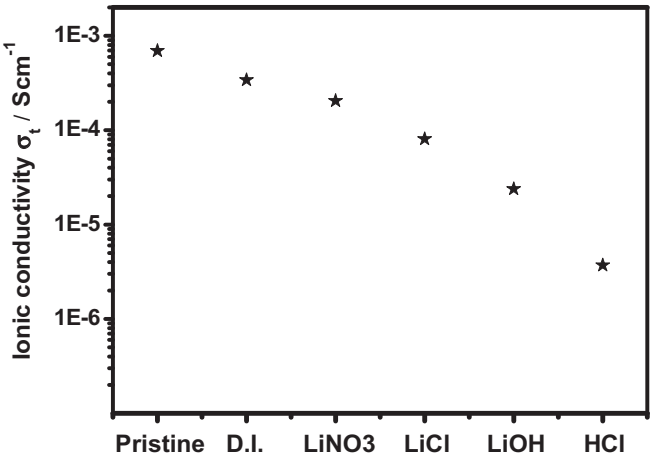

Fig. 10. Total ionic conductivity plots (σ_t) for (1) pristine $B_{0.05}$ – 825 °C for 5 h and $B_{0.05}$ specimens immersed in (2) distilled water, (3) $LiNO_3$, (4) LiCl, (5) LiOH and (6) HCl at 25 °C for 3 weeks.

Table 3
Ionic conductivity of $B_{0.05}$ glass ceramic after immersion for 3 weeks in distilled water and various aqueous solutions at 25 °C. pH of each solution is also indicated.

Solution (M)	pH	Total ionic conductivity at 25 °C (S cm^{-1})
Distilled water	7	3.4×10^{-4}
1 M $LiNO_3$	6	2.05×10^{-4}
1 M LiCl	6	8.06×10^{-5}
1 M LiOH	14	2.39×10^{-5}
0.1 M HCl	1	3.7×10^{-6}

The ionic conductivity of pristine $B_{0.05} = 6.9 \times 10^{-4}$ S cm^{-1}.

ceramic was slightly degraded after immersion in deionized water, $LiNO_3$ and LiCl solutions, while the conductivity of the glass ceramic was decreased by an order after immersion in LiOH and HCl solutions.

4. Conclusion

Pristine lithium aluminium germanium phosphate (LAGP) based lithium-ion conductors and B_2O_3 added LAGPs were successfully prepared by the melt quenching method. The crystallization temperature of LAGP decreased with the addition of B_2O_3. The addition of a small amount of B_2O_3 to the mother LAGP glass ceramic resulted in the increase in total ionic conductivity of the LAGP. The highest conductivity of 6.94×10^{-4} S cm^{-1} was achieved at 25 °C for 0.05 wt% B_2O_3 added LAGP specimen crystallized for 5 h at 825 °C. The nonlinearity in the Arrhenius total conductivity plots was observed. This nonlinearity is attributed to the presence of impurity phases $AlPO_4$ and Li_2O. The stability test of the 0.05 wt% B_2O_3 added LAGP glass ceramic revealed that the B_2O_3 added glass ceramic can be used in neutral and weak alkaline/acidic media but not in strong acid or alkaline media.

Acknowledgements

This research was supported by the MSIP(Ministry of Science, ICT & Future Planning), Korea, under the C-ITRC (Convergence Information Technology Research Center) support program (NIPA-2013-H0301-13-1009) supervised by the NIPA(National IT Industry Promotion Agency). This work was also supported by National Research Foundation of Korea (NRF) grant funded by the Korea government (MEST) (No. 2009-0085441 and No. 2012R1A2005977).

References

[1] J.M. Tarascon, M. Armand, Nature 414 (2001) 359.
[2] P.G. Bruce, S.A. Freunberger, L.J. Hardwick, J.M. Tarascon, Nat. Mater. 11 (2012) 19.
[3] J. Fergus, J. Power Sources 195 (2010) 4554.
[4] H. Nakano, K. Dokko, J. Sugaya, T. Yasukawa, T. Matsue, K. Kanamura, Electrochem. Commun. 9 (2007) 2013.
[5] F. Croce, F. Serraino Fiory, L. Persi, B. Scrosati, Electrochem. Solid State Lett. 4 (2001) A121.
[6] K. Takada, M. Tansho, I. Yanase, T. Inada, A. Kajiyama, M. Kouguchi, S. Kondo, M. Watanabe, Solid State Ionics 139 (2001) 241.
[7] T. Abe, M. Ohtsuka, F. Sagane, Y. Iriyama, Z. Ogumi, J. Electrochem. Soc. 151 (2004) A1950.
[8] T. Konishi, K. Tadanaga, M. Tatsumisago, Solid State Ionics 177 (2006) 2737.
[9] C.R. Mariappan, M. Gellert, C. Yada, F. Rosciano, B. Roling, Electrochem. Commun. 14 (2012) 25.
[10] M. Kotobuki, Y. Isshiki, H. Munakata, K. Kanamura, Electrochim. Acta 55 (2010) 6892.
[11] J. Fu, Solid State Ionics 104 (1997) 191.
[12] J. Thokchom, B. Kumar, J. Power Sources 185 (2008) 480.
[13] Y. Masuda, M. Nakayma, M. Wakihara, Solid State Ionics 178 (2007) 981.
[14] G. Adachi, N. Inamaka, H. Aono, Adv. Mater. 8 (1996) 127.
[15] J. Thokchom, B. Kumar, J. Am. Ceram. Soc. 90 (2007) 462.
[16] J.K. Feng, L. Lu, M.O. Kai, J. Alloys Compd. 501 (2010) 255.
[17] M. Kotobuki, in: 2nd International Conference on Electrical and Civil Engineering (ICEECE'2012) Singapore, April 28–29, 2012.
[18] K.C. Kang, Ceramic Engineering for Dielectrics, Taekwang Publishing Co., Seoul, Korea, 1994, p. 266.
[19] G.H. Maber, in: Proceeding of the 27th Electronic Components Conference (Arlington, VA, May 1997), Institute of Electrical and Electronics Engineers, New York, 1997, p. 391.
[20] S.H. Moon, J.H. Kim, H.Y. Chu, M. Yuri, M.H. Jeong, J.S. Choi, L.A. Oleg, U.S. Patent No. US 2012/0231349 A1, 2012.
[21] J.B. Lim, S. Nahm, H.T. Kim, J.H. Kim, J.H. Paik, H.J. Lee, J. Electroceram. Soc. 17 (2006) 393.
[22] J.S. Thokchom, B. Kumar, J. Power Sources 195 (2010) 2870.
[23] B. Kumar, J.S. Thokchom, J. Am. Ceram. Soc. 90 (2007) 3323.